Appl. Phys. B 70 [Suppl.], S149–S153 (2000) / Digital Object Identifier (DOI) 10.1007/s003400000314

Applied Physics B
Lasers
and Optics

Contrast and phase characterization of a high-peak-power 20-fs laser pulse

M. Aoyama, A. Sagisaka, S. Matsuoka, Y. Akahane, F. Nakano, K. Yamakawa

Advanced Photon Research Center, Kansai Research Establishment, Japan Atomic Energy Research Institute, Umemidai 8-1, Kizu, Kyoto 619-0215, Japan (Fax: +81-774/71-3316, E-mail: yamakawa@apr.jaeri.go.jp)

Received: 4 October 1999/Revised version: 10 March 2000/Published online: 24 May 2000 –

Abstract. We fully characterize a high-peak-power, ultrashort laser pulse in a Ti:sapphire chirped-pulse amplification laser system. The contrast, temporal, and spectral phases of the 20-fs pulse are determined by using high-dynamic-range cross-correlation and frequency-resolved optical gating techniques. Minimization of the total phase error can be achieved by balancing the phase terms of the group delay dispersion and quartic. The laser system is currently being applied to perform high-field atomic ionization experiments at $10^{20}\,\mathrm{W/cm^2}$.

PACS: 32.00; 42.60

The application of chirped-pulse amplification (CPA) to optical pulses has led to the ability to reach extremely high peak powers. Such high-peak-power ultrashort pulse lasers can realize pulses with a peak intensity of $> 10^{20}\,\mathrm{W/cm^2}$ [1] and are therefore useful for a variety of high-field applications such as the generation of ultrafast X-ray radiation [2–4] and high-harmonic generation [5, 6] from solid targets and photoionization-pumped X-ray lasers [7, 8]. A fundamental consequence of CPA in which pulse expander and amplifier components are used to stretch and amplify a seed pulse, is the presence of a pedestal or prepulse upon compression due to phase distortions. The ultrashort laser pulses may, in general, also have amplified spontaneous emission (ASE) background associated with the main laser pulse. In a laser-produced plasma experiment, such a pedestal and/or ASE would create a low-density plasma in advance of the main laser pulse and thus significantly alter the physics of the laser/plasma interaction [9]. Therefore detailed characterization and control of the temporal shape and phase of the laser pulse is crucial to the study of high-intensity physics experiments.

Techniques for the measurement of high-intensity ultrashort laser pulses are now widely used [10–12]. The frequency-resolved optical gating (FROG) technique can measure the intensity and phase of the pulse over a wide range of wavelengths using nonlinear optical materials [13]. The second-harmonic generation (SHG) FROG technique is simple to set up and can measure pulses as short as 4.5 fs in duration [14]. Delong et al. demonstrated the high-dynamic-range measurement capability of the SHG-FROG technique [15]. They showed that the noise level of the retrieved pulse is roughly of the order of 10^{-4}. The dynamic range of this method is usually limited by the detection system such as a CCD camera which is not sufficient to measure much higher contrast pulses.

A slow-scanning high-dynamic-range second-order autocorrelation has enough temporal resolution (≈ 0.5 fs) and dynamic range ($\approx 10^{12}$) [16] suitable for the detection of very low intensity ASE. Unfortunately, this technique gives information on the symmetry of the pulse shape. On the other hand, a high-dynamic-range third-order cross-correlation between the fundamental and its second-harmonic pulse, can distinguish prepulses from postpulses [17, 18]. The time resolution is, however, limited by the broadening of SHG and third-harmonic generation (THG) caused by group velocity dispersion (GVD), group velocity mismatch (GVM), and spectral filtering in the doubling and tripling crystals. For this reason the cross-correlation technique is not suitable to measure pulses with a pulse duration of the order of 20 fs. In order to fully characterize the contrast, pulse duration, and phase of 20-fs laser pulses, it is therefore necessary to use cross-correlation and SHG-FROG techniques simultaneously.

In this paper, we characterize a high-peak-power 20-fs laser pulse. The contrast and phase of the laser pulse were measured with the techniques of high-dynamic-range third-order cross-correlation and SHG-FROG. The measured contrast (defined as the ratio of the peak pulse intensity to ASE) of the pulse is of the order of 10^{-6}. The result of the phase measurement of the pulse indicates that the predominant phase distortion is quartic. We then calculate the total phase of the laser system by changing the conditions of the separations and incidence angles of the gratings in the compressor. We find that minimization of the phase distortion of the

system by balancing the phase terms of the group delay dispersion (GDD) and quartic improves the pre- and post-pulse contrast ratio.

1 SHG-FROG measurement

In this experiment we used a part of our Ti:sapphire CPA laser system operating at a 10 Hz repetition rate [1, 19, 20]. A laser pulse is generated from a Ti:sapphire oscillator with a pulse duration of ≈ 10 fs [21]. The pulse was stretched to > 1 ns in an expander and amplified by regenerative and multipass amplifiers. The output energy of the amplified pulse was ≈ 250 mJ. The separation and incidence angle of the compressor gratings were 115.219 cm and 62.97°, respectively. After the compressor, the phase of the compressed pulse was measured by using the SHG-FROG technique.

The setup of the FROG is similar to the single-shot second-order autocorrelator [1]. The nonlinear material used in the autocorrelator was a 100-μm-thick KDP crystal. The SHG signal was detected by an imaging spectrometer (Acton Research Corporation: SP-150-S) with a grating of 300 groove/mm and a CCD camera (Prinston Instruments: TE/CCD-512-TKM/1PI – 512×512 pixels). A 250-mm relay lens focused the SHG signal onto the entrance slit of the spectrometer. The magnification of the image is 1 : 0.8. The sensitivity as a function of the wavelength of the detection system was calibrated by using a halogen lamp (Ushio: JPD-100-500CS). The measured FROG trace was extracted using the central 256×256 pixel area of the CCD camera and then retrieved until the FROG error decreased to less than ≈ 0.01. The number of iterations was 20 in this case. Figure 1a shows the pulse intensity and phase in time retrieved from the SHG-FROG trace. The pulse duration is 20 fs full width at half maximum (FWHM) accompanied with pre- and post-pulses. The intensity and phase of the pulse in frequency are also shown in Fig. 1b. The spectral width is 67 nm FWHM. The duration of the transform-limited pulse calculated from the measured spectrum is 16.5 fs. The measured pulse therefore contains phase distortions.

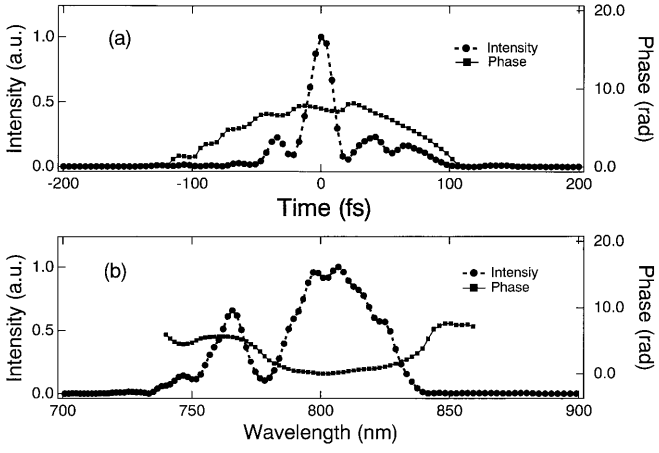

Fig. 1a,b. Retrieved intensities and phases of the SHG-FROG trace for the compressed pulse. **a** Pulse intensity (*circles*) and phase (*squares*) in time. **b** Spectral intensity (*circles*) and phase (*squares*) as a function of wavelength

The spectral phase of $\phi_{(\omega)}^{\mathrm{FROG}}$ is expressed by

$$\phi_{(\omega)}^{\mathrm{FROG}} = \phi_{(\omega)}^{\mathrm{Exp}} + \phi_{(\omega)}^{\mathrm{Amp}} + \phi_{(\omega)}^{\mathrm{Comp}}, \tag{1}$$

where ω is the angular frequency, $\phi_{(\omega)}^{\mathrm{Exp}}$ is the phase of the expander, $\phi_{(\omega)}^{\mathrm{Amp}}$ is the phase of the amplifiers, and $\phi_{(\omega)}^{\mathrm{Comp}}$ is the phase of the compressor. The phase can be represented by a Taylor's series expansion as

$$\begin{aligned}\phi(\omega) = \phi(\omega_0) &+ \left.\frac{\partial\phi}{\partial\omega}\right|_{\omega_0}(\omega-\omega_0) + \frac{1}{2!}\left.\frac{\partial^2\phi}{\partial\omega^2}\right|_{\omega_0}(\omega-\omega_0)^2 \\ &+ \frac{1}{3!}\left.\frac{\partial^3\phi}{\partial\omega^3}\right|_{\omega_0}(\omega-\omega_0)^3 + \frac{1}{4!}\left.\frac{\partial^4\phi}{\partial\omega^4}\right|_{\omega_0}(\omega-\omega_0)^4 + \dots,\end{aligned} \tag{2}$$

where ω_0 is the central frequency of the expansion. In (2), each term of phase distortion was determined by polynomial fitting to the spectral phase of the FROG measurement. The zeroth and first-order phase terms do not contribute to the change of the pulse duration. The measured pulse contains a GDD of 2.83×10^2 fs^2, a cubic phase of 3.73×10^3 fs^3, and a quartic phase of 3.80×10^6 fs^4. Based on these results, we conclude that the predominant phase distortion is quartic.

2 Minimizing of total phase error

With the goal being to obtain the shortest pulses, the compressor must compensate for all of the dispersion of the amplified pulse. A Treacy-type compressor [22], can compensate for phase distortion up to third order by changing the separations and incidence angles of the compressor gratings. Exact cancellation up to fourth order is desired to obtain ultrashort pulses (≤ 20 fs) [23]. Fittinghoff et al. suggested that balancing different phase terms can minimize the overall dispersion of the system [24]. Bagnoud et al. showed theoretically that a global optimization also improves the overall dispersion by minimizing the fourth order by some second order [25]. In their simulation, an optimization algorithm is used to find the best setting for as many variables as experimentally available. We then apply this to the experimental result of SHG-FROG measurement for the total phase simulation.

The modified total phase of $\phi_{(\omega)}^{\mathrm{Mod}}$ is determined from the experimental result of $\phi_{(\omega)}^{\mathrm{FROG}}$ by

$$\phi_{(\omega)}^{\mathrm{Mod}} = \left(\phi_{(\omega)}^{\mathrm{FROG}} - \phi_{(\omega)}^{\mathrm{Comp}}\right) + \phi_{(\omega)}^{\mathrm{CompN}}, \tag{3}$$

where $\phi_{(\omega)}^{\mathrm{CompN}}$ is the phase term introduced by the new compressor. In (3), the phase term $\phi_{(\omega)}^{\mathrm{FROG}} - \phi_{(\omega)}^{\mathrm{Comp}}$ obtained from (1) represents the phase including the expander and amplifier components in the laser system. We calculate the modified total phase as a function of $\omega - \omega_0$ for various settings of the separations and incidence angles for the new compressor gratings. The values of the root mean square (RMS) and the peak to valley of the modified total phase as a function of $\omega - \omega_0$ are also calculated for each setting. Figure 2a shows the experimental result of spectral phase (circle) which is the measured value as shown in Fig. 1b and modified total phases (solid and dashed lines). Minimization of the modified total

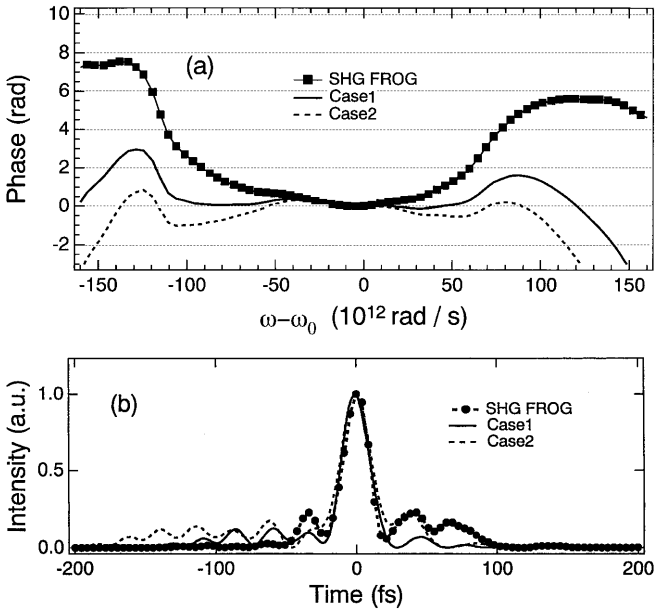

Fig. 2. a Measured and calculated total phases as a function of $\omega-\omega_0$. **b** Pulses are calculated from the Fourier transform of the measured spectrum and its phase from (**a**)

phase error can be achieved by balancing the phase terms of the GDD and quartic. Two cases are found in order to make the modified total phase as flat as possible. The separations and incidence angles of the compressor gratings of the two cases correspond to 115.192 cm, 62.95° (case 1: solid line) and 115.179 cm, 62.94° (case 2: dashed line), respectively. In case 1 the RMS of the modified total phase as a function of $\omega-\omega_0$ is minimized. In case 2 the peak to valley of the modified total phase as a function of $\omega-\omega_0$ is minimized. In Fig. 2b, each of the pulses is calculated from the Fourier transform of the measured spectrum and its phase shown in Fig. 2a. As a result, case 1 is better in terms of the reduction of pre- and post-pulses than case 2, although the pulse durations of these three cases are almost unchanged. The level of the prepulse occurring ≈ 35 fs before the main pulse using the parameters of case 1 can be reduced to below half that of the experimental value (SHG-FROG). More precise control of the total phase can also be realized by using an active phase compensator. For example, a deformable mirror can be used for an ultrashort-pulse laser system as an active phase compensator [26].

3 High dynamic range measurement

The experimental setup for the high-dynamic-range third-order cross-correlator is shown in Fig. 3. The arrangement of the cross-correlator is that of a type-I phase-matched, non-collinear geometry which incorporates SHG and THG nonlinear crystals. The SHG and THG signals were obtained with 1-mm- and 500-μm-thick KDP crystals, respectively. To minimize the dispersion of the SHG signal, reflective optics are used after frequency doubling. The two beams were focused onto the THG crystal with an aluminum-coated concave mirror ($R = 500$ mm) and had a crossing angle of 8°. In the case of nonlinear phase matching, the interaction length of the fundamental and its second-harmonic pulse becomes less than the thickness of the THG crystal. By using a slit, a Brewstar prism, and three dielectric mirrors centered at 266 nm, the cross-correlation signal was divided from the noise arising from the scattering of the fundamental and its second-harmonic pulse on the surface of the THG crystal. The THG signal was then recorded by a standard photomultiplier tube (PMT, Hamamatsu: H6780-06). A computer-controlled stepping-motor (Newport: M-UTM50PP) was used to vary the delay between the two cavity arms (up to ±160 ps). Calibrated neutral-density filters were also used to obtain the THG signals at a different attenuation level. The signal from the PMT was time gated (50 ns) to avoid any other long-term noise and averaged over ten laser shots in a Boxcar integrator (Stanford Research Systems: SR250).

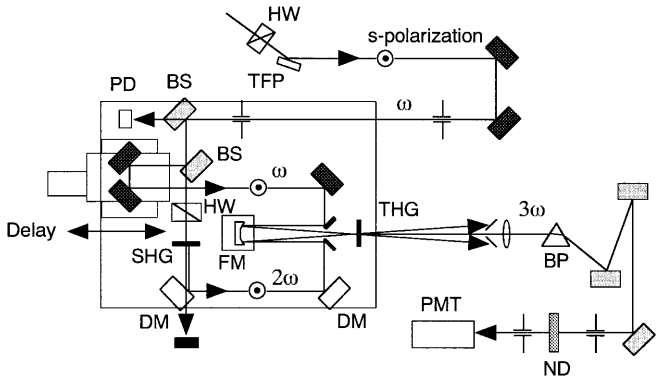

Fig. 3. Experimental setup for the high-dynamic-range third-order cross-correlator. HW: half waveplate; TFP: thin-film polarizer; BS: beam splitter; DM: dichroic mirror; PD: photodiode; FM: focusing mirror; BP: Brewster prism; ND: neutral-density filter; PMT: photomultiplier tube

The cross-correlation signal of the compressed pulses is shown in Fig. 4. Each point of cross-correlation trace with a time resolution of 670 fs corresponds to an average of ten laser shots. The detection limit of this apparatus is approximately 10^{-8}. The measured contrast is of the order of 10^{-6} limited by ASE mainly coming from the regenerative amplifier. ASE can be easily suppressed by two orders of magnitude by using a solid-state saturable absorber with a preamplifier before the pulse expander [27].

Figure 5 shows the same trace at a time scale (±1 ps) different from Fig. 4. The time resolution is about 80 fs due to GVM in the doubling and tripling crystals. The retrieved pulse obtained from the SHG-FROG measurement and the compressed pulse calculated from a Fourier transform of the measured spectrum are also shown in this figure. The cross-

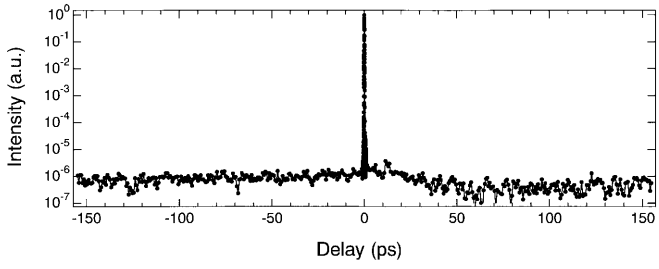

Fig. 4. High-dynamic-range cross-correlation trace of a compressed pulse. Each point of the cross-correlation trace corresponds to an average of ten laser shots

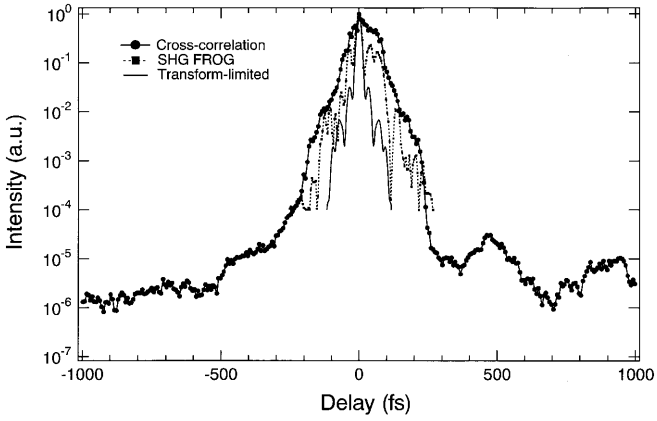

Fig. 5. High-dynamic-range cross-correlation trace which is the same trace at a time scale different from Fig. 4. SHG-FROG trace and transform-limited pulse calculated from the measured spectrum are also shown

correlation and FROG results are in good agreement at 10^{-4} which is limited by the dynamic range of the CCD camera used for the FROG measurement. In comparison with the transform-limited pulse, the leading and trailing edges of the cross-correlation signal contain a much larger pedestal within the 300-fs time scale due to quartic phase distortion as described in the previous section. This kind of pedestal can be suppressed by using the active phase compensator.

4 High-field atomic ionization experiments

In high-field physics experiments, the peak intensity is one of the most important issues for studying light–matter interaction in the relativistic regime. In general, a focused intensity can be estimated by measuring the energy, pulse duration, and spot size of the laser pulse. For example, a Gaussian spatial profile is assumed and the peak intensity is estimated as $0.61\,E/(\tau\pi r^2)$, where E is the laser energy, τ is the pulse duration (FWHM), and r is the radius of the spot size (half width at half maximum: HWHM). It should be noted that the spatial beam quality of our 100-TW laser system is determined by focusing the attenuated output with a 3-m-focal-length spherical mirror and measuring the spot size at the focus with a CCD camera. The spatial quality was about 2 and 2.5 times diffraction-limited in vertical- and horizontal-planes, respectively. Estimation of the focused intensity, however, is uncertain by a factor of $2-3$, because the full energy in the experiment is not always concentrated in the central portion of the spatial and temporal profiles. Overestimation is usually anticipated, so the effective peak intensity can be determined from the ionization rate of Ammosov–Delone–Krainov (ADK) theory [28]. Ionization in a strong laser field has been investigated extensively, and for many gases and various wavelengths the intensity dependence of the ion yield has been observed and compared with the calculated dependence. Augst et al. reported experimentally that below $10^{18}\,\mathrm{W/cm^2}$ the observed ion-production curves of noble gases agree with curves predicted by ADK theory and barrier suppression ionization [29]. Figure 6 shows the ion population of neon calculated by ADK theory as a function of the peak intensity for a pulse duration of 20 fs. From this calculation,

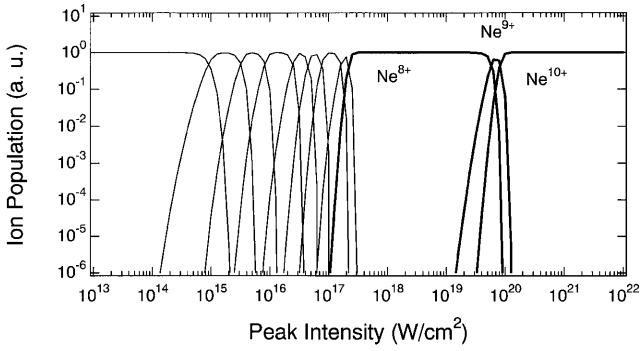

Fig. 6. Calculated ion population of the neon atom as a function of the peak intensity. The *thin solid lines* represent the populations from neutral neon to Ne^{7+}, and the *thick solid lines* represent Ne^{8+}, Ne^{9+}, and Ne^{10+}, respectively

Ne^{8+} can be produced at a peak intensity of $3\times10^{17}\,\mathrm{W/cm^2}$ defined as $\int W^{\mathrm{ADK}}\mathrm{d}t = 1$, where W^{ADK} is the ionization rate of ADK theory. Using the peak intensity at which Ne^{8+} occurs as a base, we can characterize the peak intensity well over $10^{18}\,\mathrm{W/cm^2}$ from the energy scaling of the laser pulse.

Fully stripped neon ion is generated over $10^{20}\,\mathrm{W/cm^2}$ and the maximum charge states of argon, krypton, and xenon correspond to Ar^{16+}, Kr^{26+}, and Xe^{36+} at this peak intensity. However, comparison of the ion yield with ADK theory has not yet been demonstrated in the ultrahigh-intensity regime ($\approx 10^{20}\,\mathrm{W/cm^2}$). Electrons oscillating in such an ultra-intense laser field are relativistic and thus this makes it possible to investigate an entirely new class of physical effects such as relativistic self-focusing of the laser pulse [30] and harmonic generation by relativistic electrons [31] in the ultrahigh-intensity laser field. In order to clarify the ionization mechanisms of an atom including the ionization rate, the 100-TW Ti:sapphire laser system is currently being applied to perform high-field atomic ionization experiments at $10^{20}\,\mathrm{W/cm^2}$.

5 Summary

We have fully characterized a high-peak-power, ultrashort laser pulse in a Ti:sapphire CPA laser system. The contrast, temporal and spectral phases of the 20-fs pulse are determined by using high-dynamic-range cross-correlation and SHG-FROG techniques simultaneously. The pulse duration is 20 fs FWHM accompanied with pre- and post-pulses resulting from the predominant quartic phase distortion. Minimization of the phase distortion of the system by balancing the phase terms of the GDD and quartic improves the pre- and post-pulse contrast ratio. The measured contrast of the pulse is of the order of 10^{-6} limited by ASE mainly coming from the regenerative amplifier. The high dynamic measurement and retrieved FROG results are in good agreement at 10^{-4} which is limited by the dynamic range of the CCD camera. High-field atomic ionization experiments will be demonstrated by using the 100-TW Ti:sapphire laser system at $10^{20}\,\mathrm{W/cm^2}$.

Acknowledgements. The authors would like to thank James Koga for his comments.

References

1. K. Yamakawa, M. Aoyama, S. Matsuoka, T. Kase, Y. Akahane, H. Takuma: Opt. Lett. **23**, 1468 (1998)
2. T. Guo, C. Rose-Petruck, R. Jimenez, F. Raksi, J. Squier, B. Walker, K.R. Wilson, C.P.J. Barty: SPIE. **3157**, 84 (1997)
3. J.D. Kmetec, C.L. Gordon III, J.J. Macklin, B.E. Lemoff, G.S. Brown, S.E. Harris: Phys. Rev. Lett. **68**, 1527 (1992)
4. J.F. Pellrtier, M. Chaker, J.C. Kieffer: Opt. Lett. **21**, 1040 (1996)
5. P. Gibbon: IEEE J. Quantum Electron. **QE-33**, 1915 (1997)
6. R. Lichters, J. Meyer-ter-Vehn, A. Pukhov: Phys. Plasmas **3**, 3425 (1996)
7. H.C. Kapteyn: Appl. Opt. **31**, 4931 (1992)
8. S.J. Moon, D.C. Eder: Phys. Rev. A **57**, 1391 (1998)
9. P.B. Corkum, F. Brunel, N.K. Sherman, T. Srinivasan-Rao: Phys. Rev. Lett. **61**, 2886 (1988)
10. J.L.A. Chilla, O.E. Martinez: Opt. Lett. **16**, 39 (1991)
11. K.C. Chu, J.P. Heritage, R.S. Grant, K.X. Liu, A. Dienes, W.E. White, A. Sullivan: Opt. Lett. **20**, 904 (1995)
12. D.J. Kane, R. Trebino: Opt. Lett. **18**, 823 (1993)
13. R. Trebino, K.W. DeLong, D.N. Fittinghoff, J.N. Sweetser, M.A. Krumbugel, B.A. Richman, D.J. Kane: Rev. Sci. Instrum. **68**, 3277 (1997)
14. A. Baltuska, M.S. Pshenichnikov, D.A. Wiersma: Opt. Lett. **23**, 1474 (1998)
15. K.W. DeLong, R. Trebino, J. Hunter, W.E. White: J. Opt. Soc. Am. B **11**, 2206 (1994)
16. LLE Review. **75**, 159 (1998) Laboratory for Laser Energetics, University of Rochester, Rochester, USA (unpublished)
17. G. Albrecht, A. Antonetti, G. Mourou: Opt. Commun. **40**, 59 (1981)
18. J.P. Chambaret, C. Le Blanc, G. Cheriaux, P. Curley, G. Darpentigny, P. Rousseau, G. Hamoniaux, A. Antonetti, F. Salin: Opt. Lett. **21**,break 1921 (1996)
19. K. Yamakawa, M. Aoyama, S. Matsuoka, H. Takuma, D.N. Fittinghoff, C.P.J. Barty: IEEE J. Sel. Top. Quantum Electron. **4**, 385 (1998)
20. K. Yamakawa, M. Aoyama, S. Matsuoka, H. Takuma, C.P.J. Barty, D.N. Fittinghoff: Opt. Lett. **23**, 525 (1998)
21. M. Aoyama, K. Yamakawa: Opt. Commun. **140**, 255 (1997)
22. E.B. Treacy: IEEE J. Quantum Electron. **QE-5**, 454 (1969)
23. B.E. Lemoff, C.P.J. Barty: Opt. Lett. **18**, 1651 (1993)
24. D.N. Fittinghoff, B.C. Walker, J.A. Squier, C.S. Toth, C. Rose-Petruck, C.P.J. Barty: IEEE J. Sel. Top. Quantum Electron. **4**, 430 (1998)
25. V. Bagnoud, F. Salin: IEEE J. Sel. Top. Quantum Electron. **4**, 445 (1998)
26. E. Zeek, K. Maginnis, S. Backus, U. Russek, M. Murnane, G. Mourou, H. Kapteyn: Opt. Lett. **24**, 493 (1999)
27. J. Itatani, J. Faure, M. Nantel, G. Mourou, S. Watanabe: Opt. Commun. **148**, 70 (1998)
28. M.V. Ammosov, N.B. Delone, V.P. Krainov: Zh. Eksp. Teor. Fiz. **91**, 2008 (1986) [Sov. Phys. JETP **64**, 1191 (1986)]
29. S. Augst, D.D. Meyerhofer, D. Strickland, S.L. Chin: J. Opt. Soc. Am. B **8**, 858 (1991)
30. C. Max, J. Arons, A. Langdon: Phys. Rev. Lett. **33**, 209 (1974)
31. E. Sarachik, G. Schappert: Phys. Rev. D **1**, 2738 (1970)